

Overview

Purpose: To gain a fundamental understanding of mechanisms underlying fragmentations, induced by collisional activation, of the C8 and N7 PAH-purine adducts that lead to isomer-specific fragment-ion abundance patterns.

Methods: Modeling by theoretical calculations: PM3 for initial characterization of the potential energies surfaces and refined by using density functional theory.

Results:

- w All fragmentations are highly endothermic. At internal energies below fragmentation, protons become mobile about the adducts.
- w Each site of proton attachment defines an entry point into series of rearrangements leading to a specific fragmentation.

Introduction

Carcinogenesis by polycyclic-aromatic hydrocarbons (PAH) begins with metabolic activation [1-4]. The activated products subsequently react with the bases of DNA, which in turn may cause misreading upon replication [5,6]. Such adducts have been isolated from *in vitro* and *in vivo* studies of DNA damage [7]. Our interests focus on adducts formed by reaction of purine bases in DNA with PAH's activated by one-electron oxidation [1,2].

Patterns of the fragmentation of these PAH-base adducts have been characterized by tandem mass spectrometry [7-10], and the fragmentation reactions of the purine bases have been studied thoroughly [11,12]. The relative abundances of the Ar-CN^+ and Ar-H^+ products serve to distinguish the C8 and N7 PAH-guanine isomers; the former is more abundant for the C8 isomer whereas the latter is for the N7 isomer. To provide an understanding of the mechanisms of the isomer-specific fragmentations is the goal of this ongoing, theoretical investigation [13].

References

1. Cavalieri, E. L.; Rogan, E. G. in *Free Radicals in Biology*; Pryor, W. A., ed.; Academic: New York, **1984**; vol. VI, pp. 323-369.
2. Cavalieri, E. L.; Rogan, E. G. *Pharmac. Ther.* **1992**, *55*, 183-199.
3. Sims, P.; Grover, P. L.; in *Polycyclic Hydrocarbons and Cancer*; Gelboin, H. V.; Ts'o, P. O. P., eds.; Academic: New York, **1981**; vol. 3, pp. 117-181.
4. Conney, A. H. *Cancer Res.* **1982**, *42*, 4875-4917.
5. Glover, P. L., ed., in *Chemical Carcinogens and DNA*; Chemical Rubber Company: Boca Raton, FL, **1979**; vols. 1 and 2.
6. Miller, E. C.; Miller, J. A. *Cancer* **1981**, *47*, 2327-2345.
7. Wellemans, J.; Cerny, R. L.; Gross, M. L. *Analyst* **1994**, *119*, 497-503.
8. RamaKrishna, N. V. S.; Gao, F.; Padmavathi, N. S.; Cavalieri, E. L.; Rogan, E. G.; Cerny, R. L.; Gross, M. L. *Chem. Res. Toxicol.* **1992**, *5*, 293-302.
9. RamaKrishna, N. V. S.; Padmavathi, N. S.; Cavalieri, E. L.; Rogan, E. G.; Cerny, R. L.; Gross, M. L. *Chem. Res. Toxicol.* **1993**, *6*, 554-560.
10. Byun, J.; Gooden, J.; Ramanathan, R.; Li, K.-M.; Cavalieri, E. L.; Gross, M. L. *J. Am. Soc. Mass Spectrom.* **1997**, *8*, 977-986.
11. Gregson, J. M.; McCloskey, J. A. *Int. J. Mass Spectrom. Ion Processes* **1997**, *165/166*, 475-485.
12. Nelson, C. C.; McCloskey, J. A. *J. Am. Chem. Soc.* **1992**, *114*, 3661-3668.

13. Giblin, D.; Gross, M. L. *Proceedings of the 48th ASMS Conference on Mass Spectrometry and Allied Topics*, **2000**, 732.
14. Stewart, J. J. P. *J Comp. Chem.* **1989**, *10*, 209-220, 221-264.
15. Chen, W.; Schlegel, H. B. *J. Chem. Phys.* **1994**, *101*, 5957-5968.
16. Shephard, M. J.; Paddon-Row, M. N. *J. Phys. Chem.* **1995**, *99*, 3101-3108.
17. Pople, J. A.; Scott, A. P.; Wong, M. W.; Radom, L. *Israel J. Chem.* **1993**, *33*, 345-350.
18. (a) Frisch, M. J.; Trucks, G. W.; Schlegel, H. B.; Scuseria, G. E.; Robb, M. A.; Cheeseman, J. R.; Zakrzewski, V. G.; Montgomery, Jr., J. A.; Stratmann, R. E.; Burant, J. C.; Dapprich, S.; Millam, J. M.; Daniels, A. D.; Kudin, K. N.; Strain, M. C.; Farkas, O.; Tomasi, J.; Barone, V.; Cossi, M.; Cammi, R.; Mennucci, B.; Pomelli, C.; Adamo, C.; Clifford, S.; Ochterski, J.; Petersson, G. A.; Ayala, P. Y.; Cui, Q.; Morokuma, K.; Malick, D. K.; Rabuck, A. D.; Raghavachari, K.; Foresman, J. B.; Cioslowski, J.; Ortiz, J. V.; Stefanov, B. B.; Liu, G.; Liashenko, A.; Piskorz, P.; Komaromi, I.; Gomperts, R.; Martin, R. L.; Fox, D. J.; Keith, T.; Al-Laham, M. A.; Peng, C. Y.; Nanayakkara, A.; Gonzalez, C.; Challacombe, M.; Gill, P. M. W.; Johnson, B.; Chen, W.; Wong, M. W.; Andres, J. L.; Gonzalez, C.; Head-Gordon, M.; Replogle, E. S.; Pople, J. A. *Gaussian 98*, Revision A.6, Gaussian, Inc., Pittsburgh PA, **1998**;
(b) Frisch, M. J.; Frisch, A. in *Gaussian 98, User's Reference*, Gaussian, Inc., Pittsburgh, PA, **1999**, and references therein.
19. Bauld, N. L. *Radicals, Ion Radicals, and Triplets*, Wiley-VCH: New York, NY, 1997, 166-169.

Acknowledgments

This research project was supported by the NIH-supported Mass Spectrometry Research Resource at Washington University (Grant No. P41RR00954-25).

This poster will be available on the web a couple weeks after ASMS.

Website: <http://www.chemistry.wustl.edu/~msf>

Methods

Theoretical Calculations: For structural and mechanistic elucidation, we have performed theoretical calculations on the $[M + H]^+$ of the isomeric C8 and N7 PAH-guanine adducts and their subsequent rearrangements, decomposition products and transition states, to characterize the associated potential energy surfaces (PES).

To facilitate the modeling, most calculations have been performed using anthracene as surrogate PAH, rather than benzo[a]pyrene (BP) or dibenzo[a,l]pyrene (DBP), to present a less formidable target for theoretical modeling. This PAH maintains critical characteristics of BP or DBP in adducts and subsequent decomposition products: ionization potentials (IP) of the PAH fragment are less than IP's of the guanine fragment; and similar attachment site geometries and reactivities (Figure 1 and Table 1).

w The PES for each isomer was scanned initially for minima and transition states by using the PM3 [14] semi-empirical algorithm. All potential minima were

verified as true local minima and screened on basis of connections to other ions along fragmentation pathways characterized by reasonable mechanisms and true transition states. The PM3 algorithm was chosen for this function on the basis of computational efficiency owing to the size of the ions.

The semi-empirical PM3 algorithm was part of the Spartan packages versions 5.01, 5.11, and 5.13 (Wavefunction, Inc.).

w Minima and transition states were refined by using density functional theory (DFT). DFT was selected for this instead of the perturbation methods of formal ab initio theory because DFT requires much less computational overhead, incorporates dynamic correlation, and has less spin contamination and associated problems [15]. Furthermore, DFT usually performs adequately giving proper geometries, energies, and frequencies, but it nevertheless may fail for certain small highly-symmetrical systems [16].

Geometries of minima and transition states were optimized in stages by using levels BLYP/3-21G and then B3LYP/6-31G(d,p) and confirmed at each stage by vibrational frequency analysis at the same level. From the last level, vibrational frequency analyses, thermal-energy corrections were calculated from scaled zero-point energies and fundamental vibrational frequencies [17] to attain standard conditions ($T = 298.15$ K, $p = 1.0$ atm). Then, single-point energies at level of B3LYP/6-311+G(2d,p) were calculated for the minima and

transition states at their final geometries, and the thermal-energy corrections were applied to the energies.

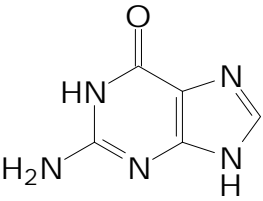
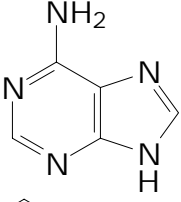
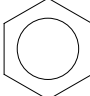
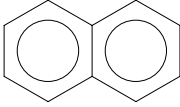
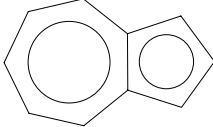
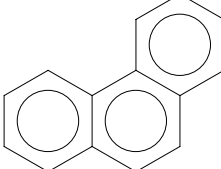
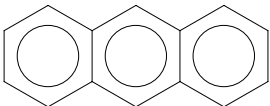
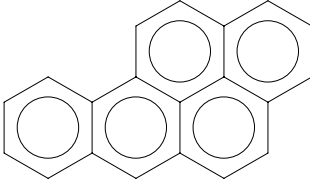
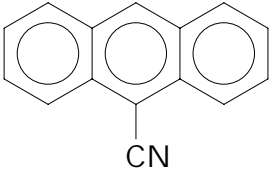
We have found that some minima, critical to previously proposed mechanisms [13], which were located by PM3 on the PES disappear at the DFT levels of geometry optimization. In addition, transition states analogous to PM3 results have been geometrically optimized by DFT but the final single-point energies have not yet been calculated. (Project is yet a work in progress!)

The DFT calculations were performed by using the Gaussian 98 (versions A.6 and A.7) suite of programs (Gaussian, Inc.) [18].

- w The results of modeling the PES surfaces are presented as relative heats of formation. The zero-point is taken as the most stable form of the adduct $[M + H]^+$ ion.
- w In addition, the potential energy surface for protonated guanine has been similarly investigated for comparison with regard to losses in common with the $[M + H]^+$ ions of the PAH adducts (data not shown).

Note: The calculations of theoretical modeling yield information about minima and transition-states on the PES, but patterns of fragmentation result from kinetic processes which are assumed to be dependent upon the points located on the PES.

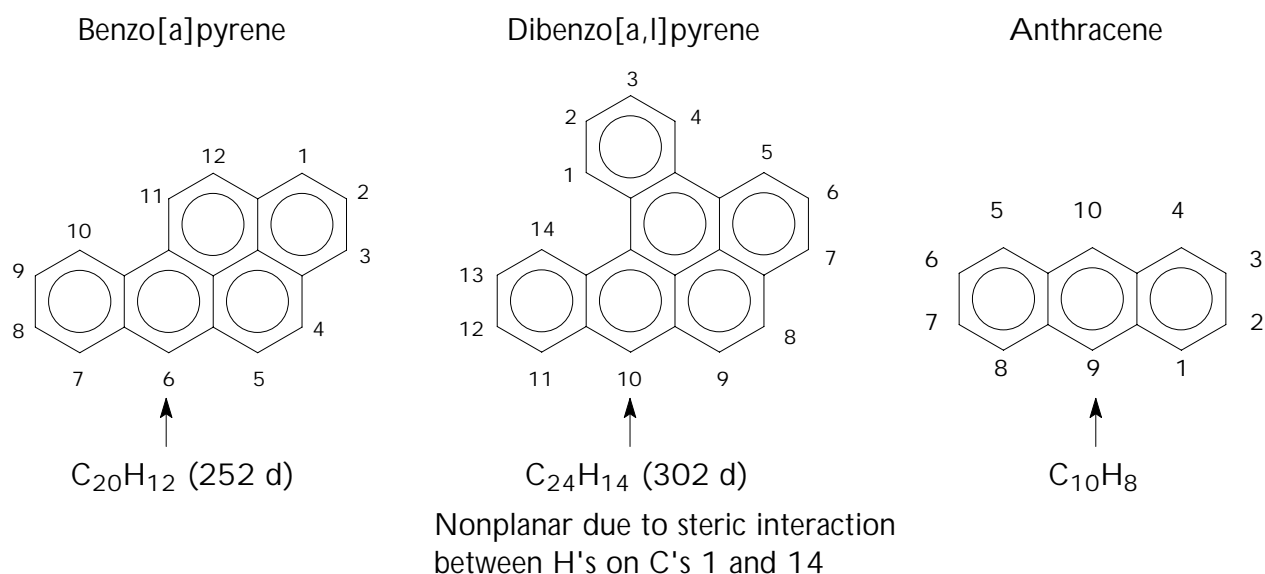
Table 1: Known Thermochemistry.

	IP(eV)	$\Delta H_f[\text{ion}]$ (kcal/mol)	$\Delta H_f[\text{neutral}]$ (kcal/mol)
	7.85	181	1
	7.80	229	49
	9.25	233	20
	8.14	224	36
	7.41	240	69
	7.89	230	49
	7.45	227	55
	7.12	233	69
	7.80	267	87

Data from: Lias, S. G.; Bartmess, J. E.; Liebman, J. F.; Holmes, J. L.; Levin, R. D.; Mallard, W. G. "Gas-Phase Ion and Neutral Thermochemistry", *J. Phys. Chem. Ref. Data*, **1998**, 17(supp. 1).

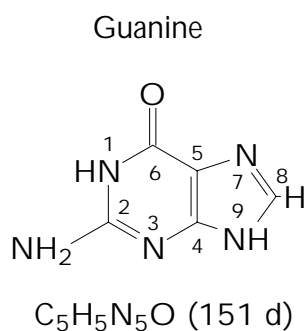
Figure 1: Reactive Sites of Components.

PAH reactive sites - One-electron oxidation



From references 1 and 2

Protonation Sites of Guanine



Site	$\Delta\Delta H$ (kcal/mol) = $-\Delta PA$
N7	0.00
O6	6.50
N3	17.69

Values were calculated by density functional theory (DFT) and are accurate with experimental data to within 3 kcal/mol

Computations from: N. Russo, M. Toscano, A. Grand, and F. Jolibois, *J. Comp. Chem.*, **1998**, *19*, 989-1000.

Results and Discussion

One-electron oxidation of the polycyclic hydrocarbons (PAH's), anthracene, benzo[a]pyrene and dibenzo[a,l]pyrene, produces radical cations with the charge localized at a unique site for each PAH, C9, C6 and C10, respectively, which become sites for efficient nucleophilic attack by the bases of DNA (Figure 1). The most abundant adducts formed include the C8- and N7-guanine isomers of the dibenzo[a,l]pyrene-guanine and benzo[a]pyrene-guanine adducts (DBP- and BP-Gau) and the N1-, N3-, N7- and N⁶-adenine isomers of DBP-Ade and the N7 and N⁶ isomers of BP-Ade. The fragmentation patterns of the $[M + H]^+$ precursors of these adducts have been studied by CAD (collisionally-activated decomposition) in our laboratory both at Washington University and the University of Nebraska [8-10]. In addition, CAD coupled with isotopic labeling to characterize the fragmentation of protonated purine bases has been reported [11,12].

Characteristic Fragmentations: The CAD spectra of $[M + H]^+$ of the isomeric C8- and N7-PAH-guanine adducts are characterized by unique features derived from the PAH moiety of the adducts:

- w The $[M + H]^+$ ions of the PAH-purine adducts, although they are even-electron, closed-shell ions, give rise to abundant fragment ions that are odd-electron, open-shell species, unlike the $[M + H]^+$ ions of the protonated purine bases. Such charge partitioning requires that the final step in the fragmentation be a single-bond cleavage and the PAH moiety possess a lower IP than the purine moiety (Table 1).
- w Many fragment ions that contain the PAH moiety are paired with additional fragment ions of $2 m/z$ less. For DBP-10- adducts, abundances of fragments having the additional loss of H_2 are significant. We suspect that relief of significant steric strain drives the loss of H_2 and formation of C1-C14 bond.

Isomer-Specific Fragmentation Patterns: Collision activation (CA) of the $[M + H]^+$ of the DBP-10- and BP-6-guanine adducts produces fragments of $ArCN^+$ or $ArNC^+$ and ArH^+ of prominent abundances, unlike protonated guanine. Fragment-ion abundances: $ArCN^+ \gg ArH^+$ for the C8 isomers, but $ArNC^+ < ArH^+$ for the N7 isomers (Table 2).

Theoretical modeling results: The potential energy surfaces for the $[M + H]^+$ ions of the C8 and N7 isomers of anthracyl-9-guanine (Anth-Gua) have been determined as described in Methods.

- w All fragmentations are highly endothermic, by >50 kcal/mol. But >70 kcal/mol of total internal energy is required to promote decomposition from the most stable form of the precursor to the most favorable products over intervening transition states. The calculated fragmentation endothermicities are ~ 12 kcal/mol lower by DFT than by PM3, reported last year [13].
- w The most favorable site for protonation of the C8-Gua isomer is N7 as it is for the free base (Figure 1). However, the N7-Gua isomer is already a preformed ion with the least basic proton site at N9.
- w At internal energies >50 kcal/mol but below that required for fragmentation, protons in the precursor ions become mobile, migrating about the ring systems (Figures 2 and 3). Some configurations accessed by the mobile protons define entry points to series of rearrangements that lead to products.
- w The decompositions, which generate $ArCN^{+\bullet}$ or $ArNC^{+\bullet}$ from the $[M + H]^+$ of the C8 and N7 isomers, take place by two step mechanisms instead of concerted cycloreversion reactions, in accord with previous reports for radical systems [19]. (There is no linking transition state for the concerted

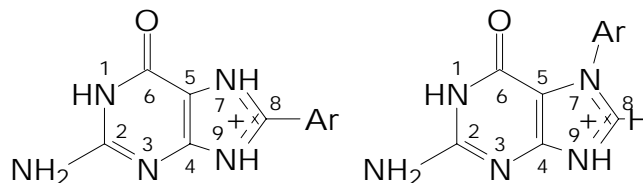
cycloreversion reaction.) The decompositions forming $\text{ArCN}^{+\bullet}$ from the C8 isomer result from proton migration to C4 or C5 of the guanine (Scheme 1a), where the routes to formation of $\text{ArNC}^{+\bullet}$ from the N7 isomer start with proton migration to C5 of the guanine and differ by when the proton is transferred from the C8 position (Scheme 2a).

- w The decompositions which give rise to the $\text{ArH}^{+\bullet}$ product from the $[\text{M} + \text{H}]^+$ of the C8 and N7 isomers in both cases arise from the migration of a proton to the C9 position of the anthracene (Schemes 1b and 2b). Note that for the proposed mechanism for the generation of $\text{ArH}^{+\bullet}$ from the N7 precursor, one of the intermediates located by PM3 becomes a shoulder without a minimum on the reaction trajectory as determined by DFT methods.
- w The proposed mechanisms for the production of $\text{ArCN}^{+\bullet}$ or $\text{ArNC}^{+\bullet}$ and $\text{ArH}^{+\bullet}$ from the $[\text{M} + \text{H}]^+$ of the C8 and N7 Anth-Gua isomers can rationalize the relative abundance distributions of these products. The rate-limiting steps in the formation of $\text{ArCN}^{+\bullet}$ from Anth-C8-Gua requires ~ 10 kcal/mol less energy than the rate-limiting step for the formation of $\text{ArH}^{+\bullet}$. Whereas for the Anth-N7-Gua isomer, the rate-limiting steps to $\text{ArNC}^{+\bullet}$ and $\text{ArH}^{+\bullet}$ favor the latter by >10 kcal/mol.
- w The final steps in all proposed mechanisms involve the cleavage of a single bond, as postulated on basis of the charge partitioning between the products.

Table 2: Fragmentation Patterns.

Fragmentation by CA of PAH-Gua Adducts

[M + H]⁺ precursors (*m/z* 452) DBP-10-C8-Gua DBP-10-N7-Gua

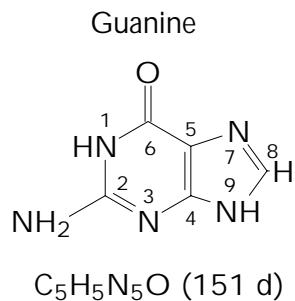


Fragment Ion	<i>m/z</i>	Rel. Abundance		Rel. Abundance
[(M + H) - NH ₃] ⁺	435	medium		medium
Ar—CN ^{+•} or Ar—NC ^{+•}	327	large	>	medium
C ₂₄ H ₁₂ N ⁺	314	small	~	small
Ar—H ^{+•}	302	small	<<	large
[(Ar—H) - H ₂] ^{+•}	300	medium	<	large
Ar ⁺	301	medium	~	medium

From reference 9. DBP-10- = dibenzo[a,l]pyrenyl-10-.

Analogous results for the benzo[a]pyrenyl-6- (BP-6-) adducts are reported in reference 8.

Fragmentation by CA of Guanine



Decomposition
of [M + H]⁺

- NH₃

- NH=C=NH
or NH₂CN

NH=C=NH₂⁺

Source

N1 and N² equally

N1-C2-N²

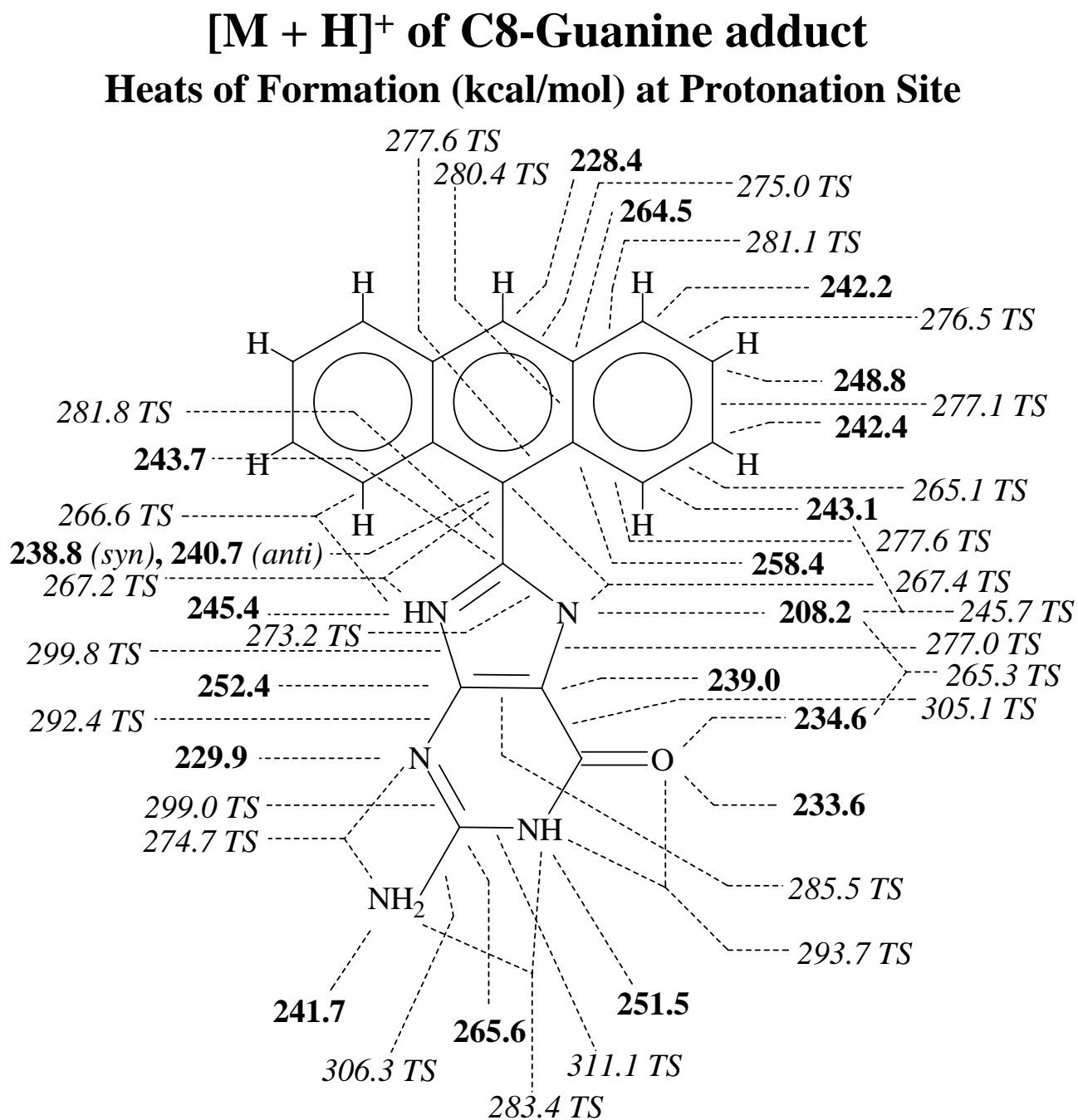
N1-C2-N²

Decompositions were determined by ¹³C and ¹⁵N labeling and comparison with mono-methylated analogs in conjunction with MS/MS.

The site of protonation is almost exclusively at N7.

Data from references 11 and 12

Figure 2: Proton Migration.



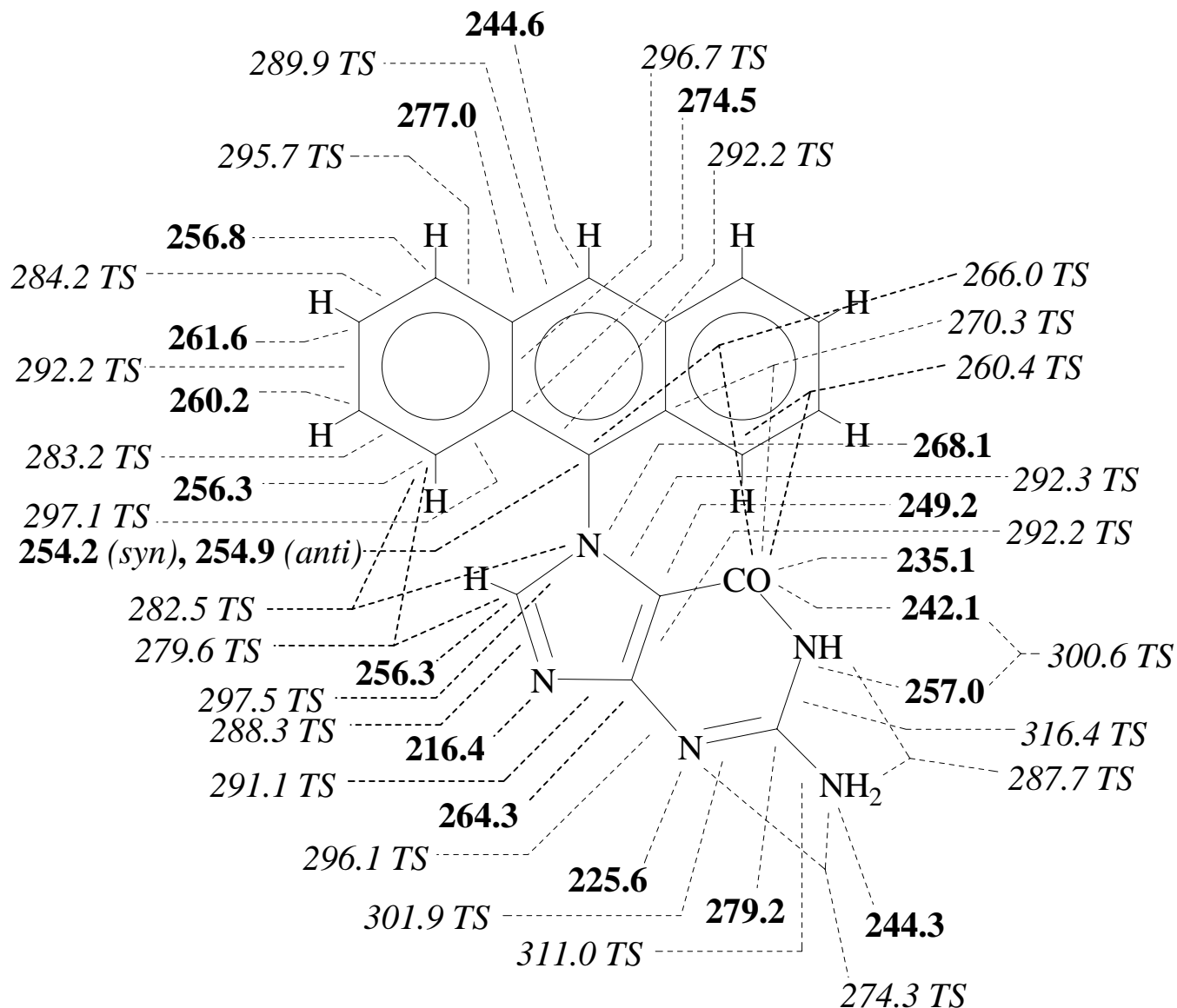
Heats of formation are given for indicated sites of proton attachment (minima) or bridging sites of transition states.

All heats of formation are presented in kcal/mol. The stationary states are indicated in **bold**, and the transition states are given by *italic TS*.

All calculations were performed by PM3 algorithm.

Figure 3: Proton Migration.

[M + H]⁺ of N7-Guanine Adduct Heats of Formation (kcal/mol) vs Protonation Site



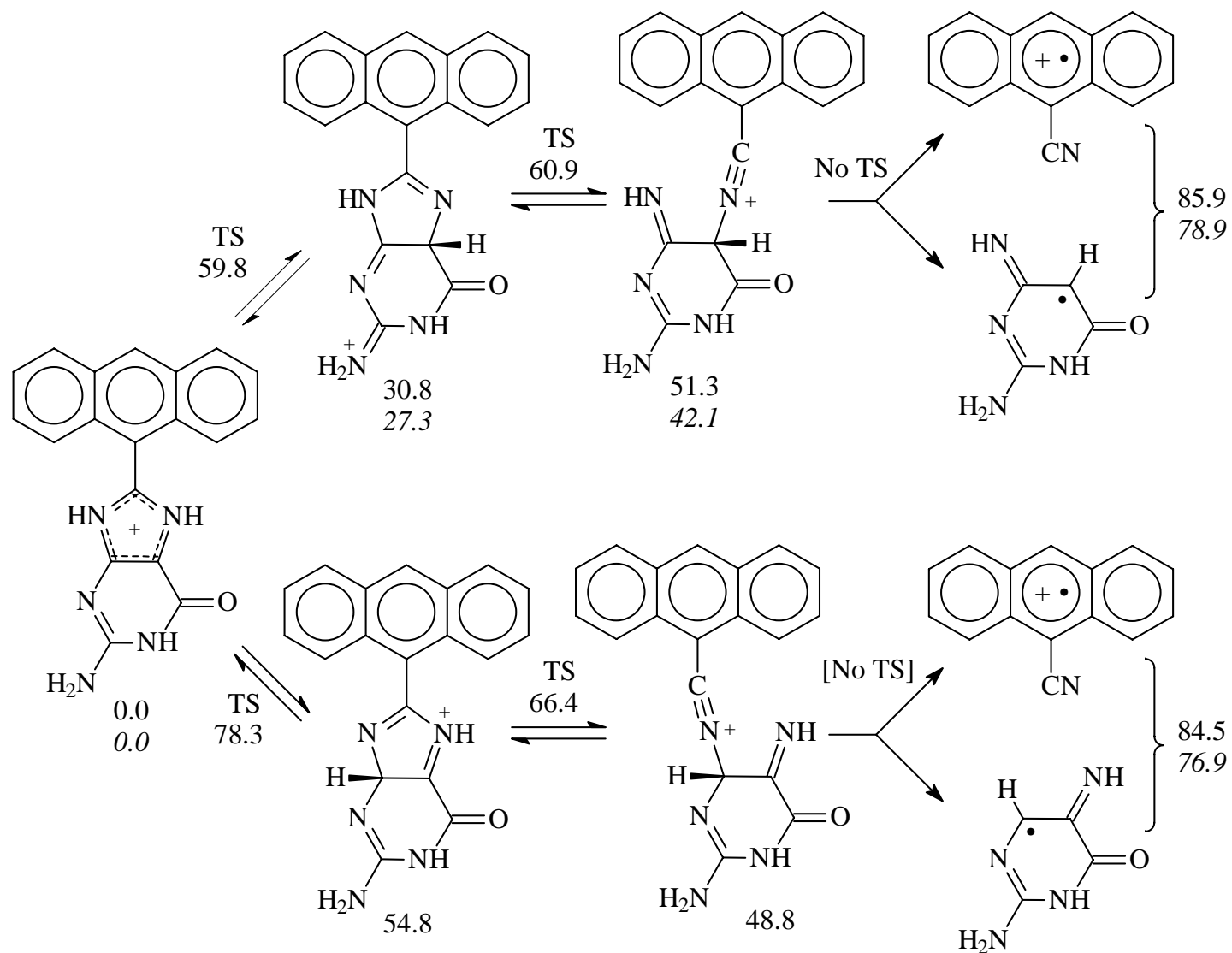
Heats of formation are given for indicated sites of proton attachment (minima) or bridging sites of transition states.

All heats of formation are presented in kcal/mol. The stationary states are indicated in **bold**, and the transition states are given by *italic TS*.

All calculations were performed by PM3 algorithm.

Scheme 1a: Proposed Fragmentation Mechanisms.

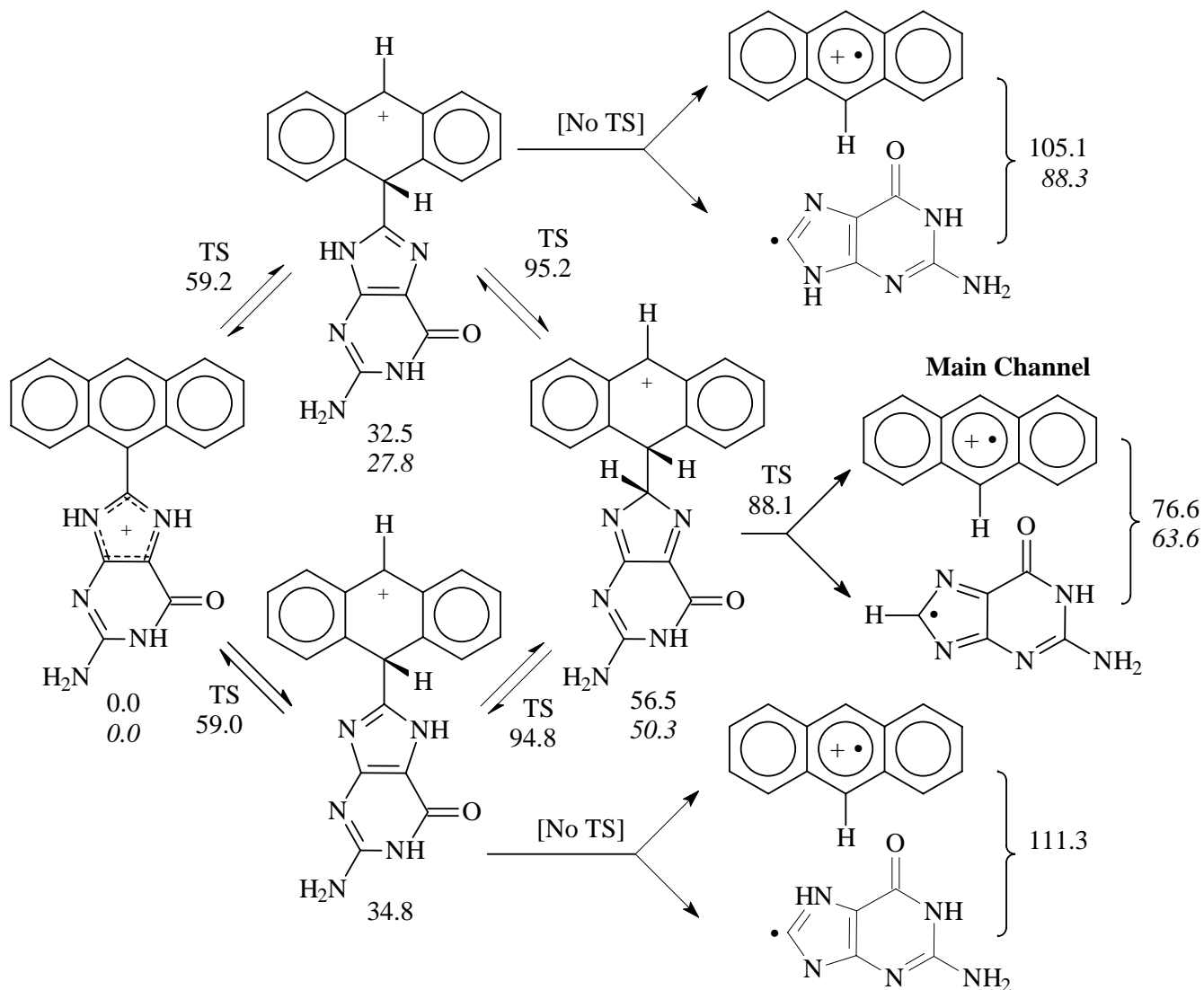
C8-Guanine adduct: Mechanism for Production of ArCN⁺



Relative heats of formation (kcal/mol); TS = transition state; states were calculated by PM3 and *DFT*: B3LYP/6-311+G(2d,p)//B3LYP/6-31G(d,p).

Scheme 1b: Proposed Fragmentation Mechanisms.

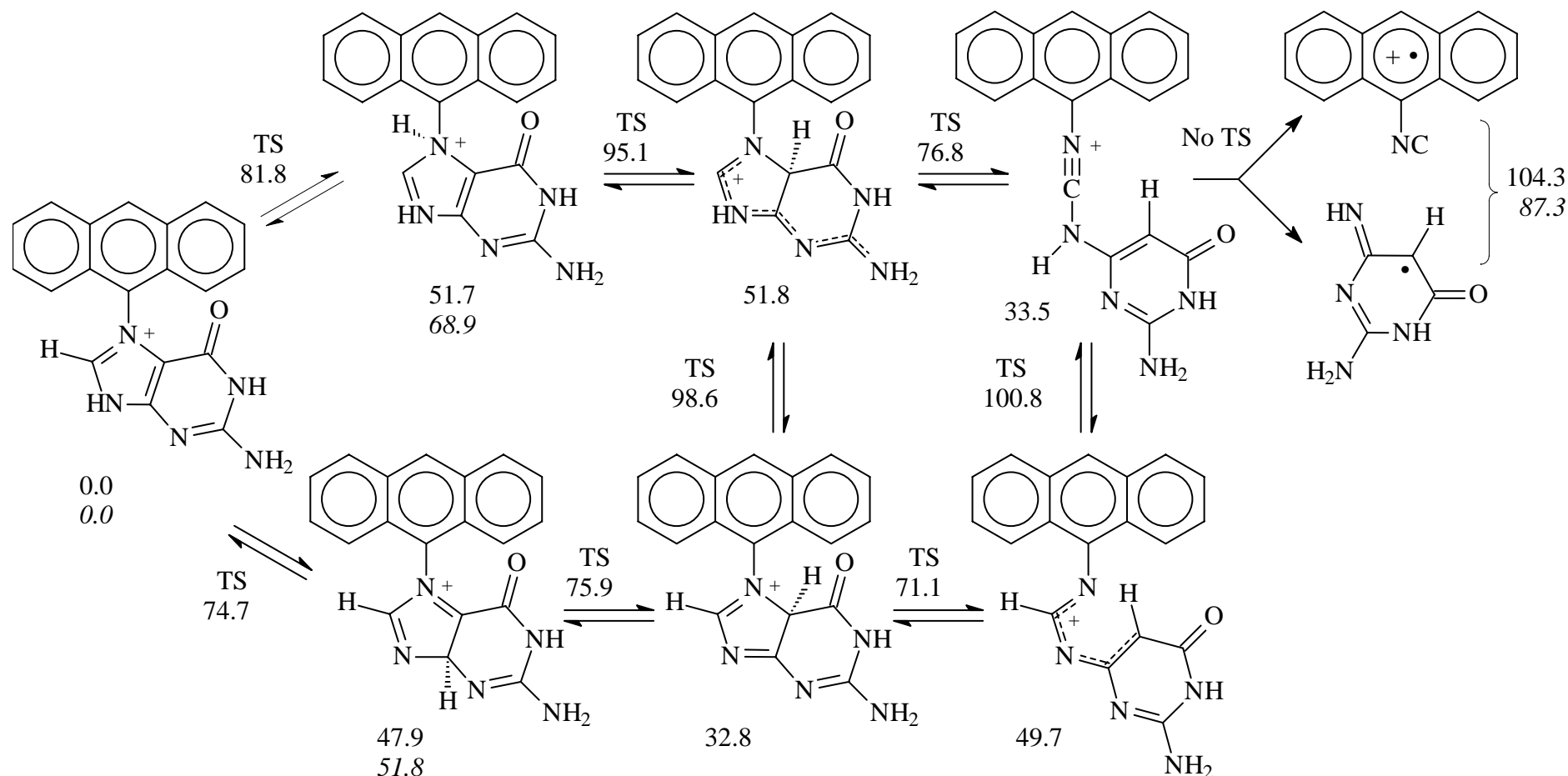
C8-Guanine adduct: Mechanism for Production of ArH⁺



Relative heats of formation (kcal/mol); TS = transition state; states were calculated by PM3 and *DFT*: B3LYP/6-311+G(2d,p)//B3LYP/6-31G(d,p).

Scheme 2a: Proposed Fragmentation Mechanisms.

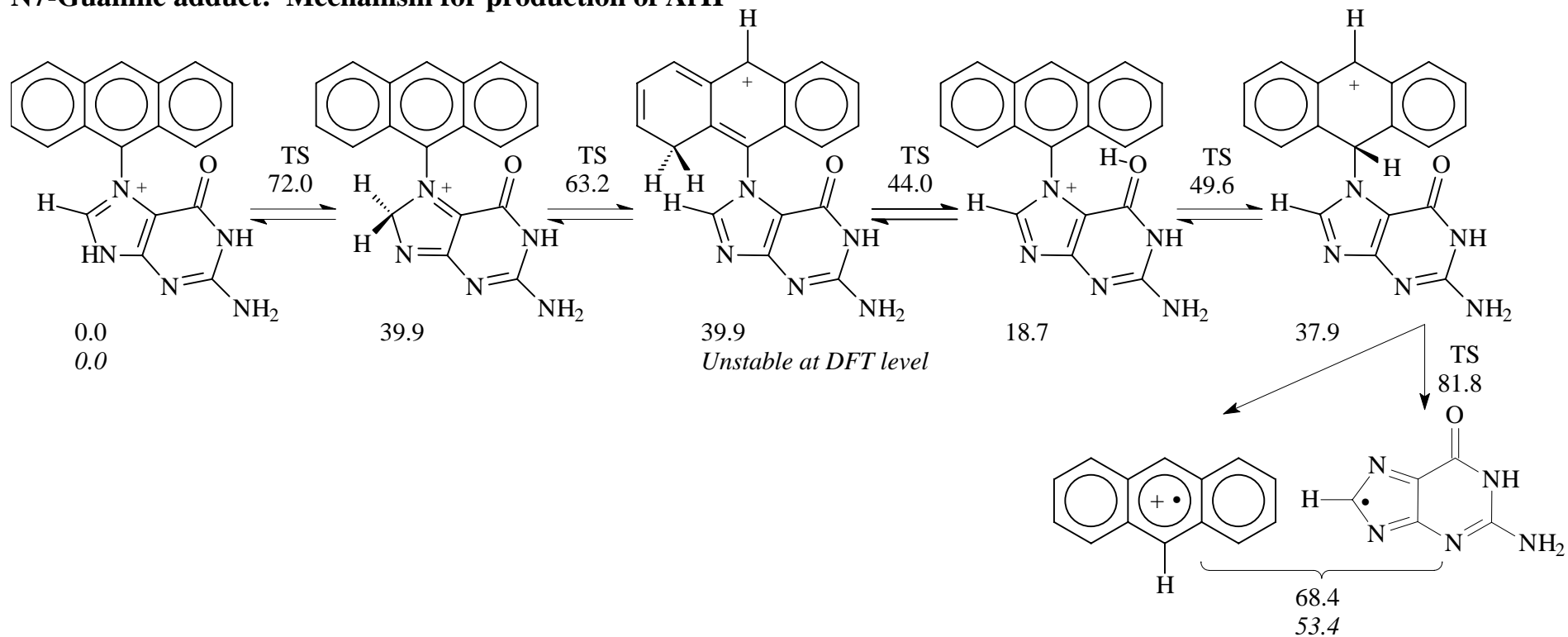
N7-Guanine adduct: Mechanism for production of ArNC⁺



Relative heats of formation (kcal/mol); TS = transition state; states were calculated by PM3 and *DFT*: B3LYP/6-311+G(2d,p)//B3LYP/6-31G(d,p).

Scheme 2b: Proposed Fragmentation Mechanisms.

N7-Guanine adduct: Mechanism for production of ArH⁺



Relative heats of formation (kcal/mol); TS = transition state; states were calculated by PM3 and *DFT*: B3LYP/6-311+G(2d,p)//B3LYP/6-31G(d,p).

Conclusions

We have applied theoretical DFT and PM3 calculations to characterize the potential energy surfaces for the generation of $\text{ArCN}^{+\bullet}$ ($\text{ArNC}^{+\bullet}$) and $\text{ArH}^{+\bullet}$ from the C8 and N7 isomers of PAH-guanine using anthracene as a surrogate PAH.

- w The fragmentations are highly endothermic by >50 kcal/mol, an energy great enough to promote proton mobility about the ring systems. Various proton attachment sites define entry points leading to fragmentation.
- w The generation of $\text{ArCN}^{+\bullet}$ or $\text{ArNC}^{+\bullet}$ from the C8- and N7-Gua adducts proceeds by two step sequential processes rather than concerted cycloreversion reactions. All final steps involve single-bond cleavage.
- w The pathway to $\text{ArCN}^{+\bullet}$ is favored by ~ 10 kcal/mol over that to $\text{ArH}^{+\bullet}$ for the C8 isomer, whereas $\text{ArH}^{+\bullet}$ formation is favored by > 10 kcal/mol over $\text{ArNC}^{+\bullet}$ generation for the N7 isomer. These results are consistent with the experimentally observed relative abundance distributions for these products.